3B.4 MICROPHYSICAL DIFFERENCES BETWEEN TORNADIC AND NONTORNADIC SUPERCELL REAR-FLANK DOWNDRAFTS REVEALED BY DUAL-POLARIZATION RADAR MEASUREMENTS

MATTHEW R. KUMJIAN* AND ALEXANDER V. RYZHKOV
Cooperative Institute for Mesoscale Meteorological Studies, University of Oklahoma, and NOAA/OAR/National Severe Storms Laboratory, Norman, Oklahoma

1. INTRODUCTION

One of the most challenging problems in severe storms research today is supercell tornadogenesis. The Verification of the Origins of Rotation in Tornadoes Experiment (VORTEX; Rasmussen et al. 1994) provided a large dataset of *in situ* and remote sensing observations of tornadic and nontornadic supercells. However, the ensuing analysis of these data revealed that tornadic and nontornadic supercell storms are virtually indistinguishable in their radar appearances at the scales resolvable in the analyses (e.g., Trapp 1999; Wakimoto and Cai 2000).

The supercell rear-flank downdraft (RFD) has been implicated in tornadogenesis for several decades (e.g., Ludlam 1963; Lemon and Doswell 1979; Brandes 1981; Davies-Jones 1982; Davies-Jones and Brooks 1993). The role of the downdraft is to transport air rich in angular momentum to the surface where it can be converged beneath the updraft. The RFD is partially observed on radar displays as a "hook echo," which has also been associated with severe weather for many years (e.g., Battan 1959). Markowski (2002) provides a comprehensive review of RFDs and hook echoes. Recently, *in situ* measurements using mobile mesonets (Straka et al. 1996) during VORTEX have shown that downdraft baroclinicity can be important. Markowski et al. (2002) and Grzych et al. (2007) present observational data suggesting that tornadogenesis appears to be sensitive to thermodynamic characteristics of the RFD. These observations show that supercells which produced significant tornadoes had RFDs with smaller equivalent potential temperature and virtual potential temperature deficits than the RFDs of nontornadic supercells. Modeling results of Markowski et al. (2003) support these findings, suggesting that excessively cold RFDs are associated with relatively weak surface convergence that cannot stretch vertical vorticity to tornadic magnitudes. Markowski et al. (2008) describe a purely baroclinic mechanism for the production of low-level vertical vorticity by a negatively-buoyant downdraft, as well as substantiating observations of the resulting arch-shaped vortex lines within the hook echo. Nonetheless, purely barotropic mechanisms can instigate tornadogenesis as well, at least in numerical models (Davies-Jones 2008).

Downdrafts can be driven dynamically through perturbation pressure gradient forces (e.g., Lemon and Doswell 1979; Rotunno and Klemp 1982; Klemp and Rotunno 1983; Wicker and Wilhelmson 1995; Wakimoto et al. 1998), through drag-induced momentum transport between the air and falling hydrometeors (e.g., Shapiro 2005 and refrences therein), and thermodynamically through the production of negative buoyancy via evaporation, melting, and sublimation of hydrometeors (e.g., Srivastava 1985, 1987). The downdraft thermodynamic characteristics are governed by the extent that these microphysical processes occur. Thus, the amount of evaporation and melting of hydrometeors in the RFD of supercells may have a significant impact on the processes associated with tornadogenesis (Markowski et al. 2002).

Conventional single-polarization radars used in VORTEX are inadequate for microphysical retrievals. However, dual-polarization radars are highly sensitive to particle phase transitions such as melting (and to a lesser extent, evaporation and sublimation). In principle, then, the effects of these microphysical processes influencing RFD thermodynamic characteristics may be apparent in polarimetric radar data from supercell hook echoes. For the first time, this study analyzes the microphysical characteristics of supercell RFDs with polarimetric radar observations. A small sample of tornadic and nontornadic supercell hook echoes is investigated in an attempt to find any systematic differences in the polarimetric properties between tornadic and nontornadic storms. Such differences are found and are physically consistent with conclusions of previous studies.

Additionally, a simple explicit bin microphysics model of evaporation of raindrops is used to support the notion that evaporation influences the observed polarimetric variables. Through theoretical and model results we will show that these differences between T and NT hook echoes are consistent with differences in evaporation rates at low levels and may be enhanced at C band due to the stronger resonance scattering effects present at smaller wavelengths.

**Corresponding author address:* Matthew R. Kumjian, 120 David L. Boren Blvd., National Weather Center Suite 4900, Norman OK 73072. Email: matthew.kumjian@noaa.gov

2. DATA AND METHODS

Data were collected by the polarimetric prototype WSR-88D in Norman, Oklahoma (hereafter KOUN). The radar variables considered in this study are the radar reflectivity factor at horizontal polarization Z_H, base Doppler velocity V_r, differential reflectivity Z_{DR}, specific differential phase K_{DP}, and the co-polar cross-correlation coefficient at zero lag time ρ_{HV}. Details about the physical interpretation of polarimetric radar variables can be found in the literature (e.g., Zrnić and Ryzhkov 1999; Straka et al. 2000; Bringi and Chandrasekar 2001; Ryzhkov et al. 2005a; Kumjian and Ryzhkov 2008).

For this analysis, 4 tornadic and 5 nontornadic supercells are analyzed. One volume scan was selected from each case based on the following criteria. For the tornadic cases, the volume scan just preceding tornadogenesis was chosen. This is to ensure that no tornadic debris was present; tornadic debris has very distinct and dominant polarimetric characteristics (Ryzhkov et al. 2005b) and is not representative of hydrometeors in the hook echo. For the nontornadic storms, the volume scan when the storm was occluding (based on the Z_H and V_r fields) and/or when the National Weather Service issued a tornado warning was selected. The lowest elevation angle not contaminated by ground clutter was used, and cases were selected such that the radar sampled the storm in the lowest 1 km as to best capture the near-surface conditions. Information about each of the cases is presented in Table 1.

Low-level (< 1 km AGL) radar data are plotted as PPIs. The data are calibrated and corrected for noise before the analysis. The hook echo is identified visually from the Z_H field (in all cases there was a well-defined hook echo or echo appendage present), and the data from the gates within the hook echo are selected. Instead of directly comparing the raw K_{DP} values to other variables such as Z_H, the rainfall rates from K_{DP} and Z_H following Ryzhkov et al. (2005a) are computed:

$$R(Z_H) = 0.017 \cdot 10^{0.0714\, Z_H} \quad (1)$$

where Z_H is in dBZ and R is in mm hr^{-1}, and

$$R(K_{DP}) = 44.0 |K_{DP}|^{0.822}\, \mathrm{sgn}(K_{DP}) \quad (2)$$

where K_{DP} is in deg km^{-1}. This is a more meaningful comparison than the raw values because $R(Z_H)$ and $R(K_{DP})$ should be well correlated in pure rainfall with R > 10 mm hr^{-1} at S band.

Date	Time (UTC)	ϕ_e	Approximate Beamheight (AGL)
8 May 2003	*2157*	*1.5°*	*693 m*
10 May 2003	*0157*	*0.5°*	*1011 m*
20 May 2003	0021	0.0°	740 m
26 May 2004	2352	0.44°	552 m
30 May 2004	*0155*	*0.0°*	*200 m*
11 April 2007	0009	0.0°	383 m
31 March 2008	*0630*	*0.48°*	*658 m*
23 April 2008	2247	1.46°	862 m
1 June 2008	0339	0.17°	872 m

Table 1: List of the cases investigated in this study. The case is categorized as tornadic (italic) or nontornadic (normal), and the time of the volume scan selected is provided (UTC). The elevation angle of the scan and the corresponding approximate beamheight is also given.

3. QUANTITATIVE ANALYSIS

Scatterplots of Z_H versus Z_{DR}, Z_H versus ρ_{HV}, and $R(Z_H)$ versus $R(K_{DP})$ for all of the tornadic and nontornadic storms are constructed (Figs. 1 – 3). In the Z_H – Z_{DR} plot (Fig. 1), it appears (despite the substantial overlap) as if the bulk of the tornadic storm Z_{DR} values may be slightly lower than the nontornadic Z_{DR} values for a given Z_H, especially for higher Z_H. In Fig. 2, tornadic ρ_{HV} points tend to display less variability than nontornadic ρ_{HV} points for Z_H > 30 dBZ. The $R(Z_H)$ – $R(K_{DP})$ plot shows little discernable difference between tornadic and nontornadic cases (Fig. 3). However, one should note that the scatter is generally *not* around the one-to-one line, as it should for most typical rain cases (e.g. Ryzhkov and Zrnić 1996; Ryzhkov et al. 2005a; Giangrande et al. 2008). In fact, a substantial number of data points from both tornadic and nontornadic storms are located below the one-to-one line, indicative of greater $R(Z_H)$ than $R(K_{DP})$, which suggests that the DSD in supercell hook echoes is skewed towards larger drops. Since the wide scatter of the data for low Z_H values in Figs. 1 – 3 may reflect the inclusion of low-level inflow and RFD gust front nonmeteorological scatterers (Kumjian and Ryzhkov 2008), only points for Z_H > 30 dBZ will be considered herein.

When analyzing the data from these cases it is evident that there exists a substantial amount of variability. Because of this significant scatter it is convenient to construct "median lines." For each 2-dBZ interval of Z_H (from 30 – 32 dBZ to 54 – 56 dBZ), the median value of Z_{DR} and ρ_{HV} are computed. The median line simply connects these computed values. To alleviate some of the case-to-case variability, the

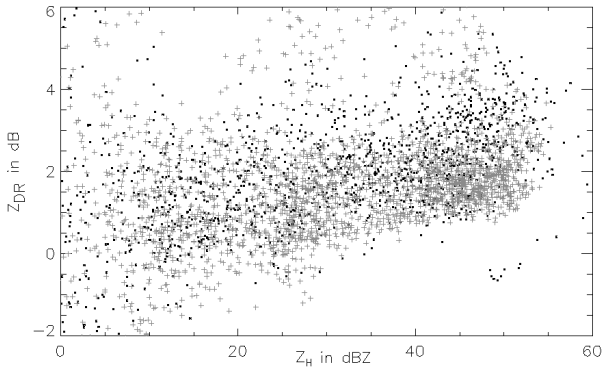

Fig. 1: Z_H vs. Z_{DR} scatterplot for tornadic hook echoes (grey crosses) and nontornadic hook echoes (black points). All nine cases are included.

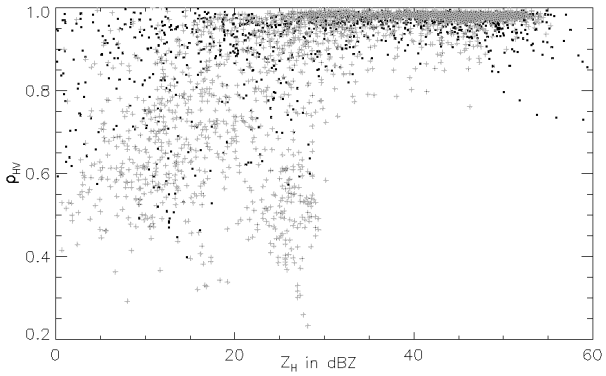

Fig. 2: As in Figure 1, except Z_H vs. ρ_{HV} is shown.

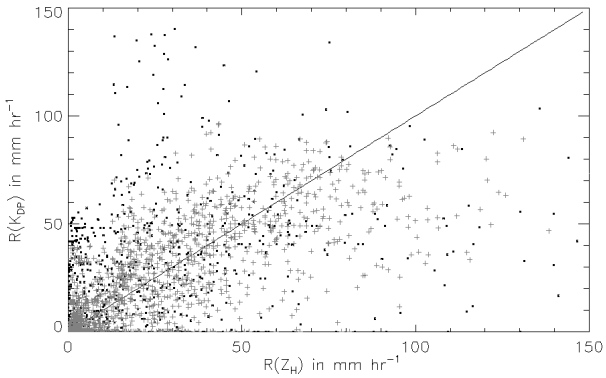

Fig. 3: As in Figure 1, except that $R(Z_H)$ vs. $R(K_{DP})$ is shown.

data from each nontornadic and each tornadic case are concatenated and median lines are produced for the aggregated nontornadic and tornadic hook echo datasets.

To illustrate the great overlap between the datasets, mean lines (constructed in an analogous manner) are indicated along with the standard deviations on either side of the mean. Although considerable overlap is evident (Fig. 4) there is evidence that a subtle separation exists between the tornadic and nontornadic datasets. The data suggest that nontornadic hook echoes are characterized by DSDs more skewed

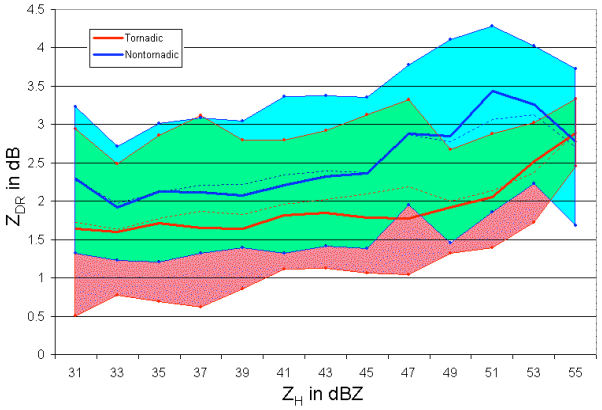

Fig. 4: Comparison of Z_H vs. Z_{DR} for tornadic and nontornadic data. The thick blue and red lines are the median lines for nontornadic and tornadic cases, respectively. The thin dashed lines are the mean lines. The thin solid lines with markers bound the interval of one standard deviation from the mean line. The distribution of tornadic data within one standard deviation of the mean is highlighted in pink, the nontornadic data in blue, and the regions of overlap in green. Despite the significant overlap (green), the distributions appear to be slightly offset.

towards larger drops than tornadic hook echoes. One possible explanation is that more vigorous evaporation occurred in the nontornadic cases than in the tornadic cases, as suggested by Markowski et al. (2002). For a given DSD, enhanced evaporation will preferentially deplete the smaller drops, causing the median drop size of the DSD to increase. This effect is further explored and quantified in the next section.

The median difference between the median Z_{DR} lines is 0.48 dB and the mean difference is 0.60 dB. Though this systematic difference is *not* statistically significant, it is at least encouraging that a difference apparently exists and that it is physically consistent with previous research and hypotheses regarding differences in tornadic and nontornadic hook echoes. However, more cases should be investigated as they become available to reduce the statistical uncertainty.

Median ρ_{HV} lines for the concatenated data exhibit a much smaller difference than the median Z_{DR} lines, one that is likely smaller than the precision of operational WSR-88D radars (Fig. 5). The median difference is 0.007 and the mean difference is 0.009. Notice that the majority of the points are found between Z_H values of 37 – 47 dBZ, where the differences between the median ρ_{HV} values are negligible. Thus, the differences may be artifacts of statistical noise. In fact, at S band in pure rain, ρ_{HV} will not drop below about 0.98, so large changes due to differences in the DSDs modified by evaporation between tornadic and nontornadic hook echoes are not expected at S band. We will elaborate on this point in a later section.

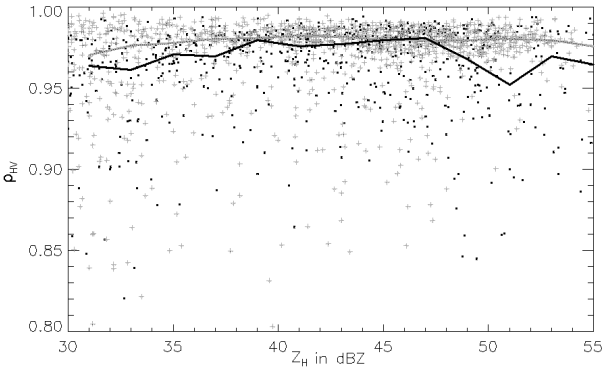

Fig. 5: Same as in Fig. 2, except the median lines for tornadic (gray) and nontornadic (black) cases are included.

To better illustrate the unusual DSD in supercell hook echoes, the median Z_{DR} lines are compared to the $Z_H - Z_{DR}$ relation found for typical Oklahoma precipitation events in Cao et al. (2008). The relation was derived from 14200 observed DSDs over a broad spectrum of precipitation regimes and is given by

$$Z_{DR} = 10^{\left(-2.6857 \cdot 10^{-4} Z_H^2 + 0.04892 Z_H - 1.4287\right)} \tag{3}$$

where both Z_H and Z_{DR} are in logarithmic scale. The supercell median lines are clearly much flatter than the Cao et al. (2008) relation (Fig. 6). The difference is especially striking for Z_H less than about 45 dBZ. Above 45 dBZ, the T median line is similar to the Cao et al. relation. All three curves tend to converge for Z_H greater than 53 dBZ, suggesting that very high-Z_H precipitation tends to be uniform across the storm spectrum.

4. EVAPORATION MODEL

To investigate the impact of evaporation on polarimetric variables, a simple bin microphysical model is constructed. The model configuration and physics are described in the next subsection, followed by a presentation of the experimental design and the model results.

4.1. Model Physics

The model tracks the independent evolution of 80 different raindrop sizes or "bins" ranging from 0.05 mm to 7.95 mm in 0.1-mm increments. Thus, no drop interactions (such as collisions, break-up, or coalescence) are considered. The drops fall through a one-dimensional domain 3 km in depth with 100-m vertical resolution with a prescribed temperature and humidity profile.

As the drops fall into a subsaturated environment, the change in drop radius r is given by

$$r\frac{dr}{dt} = \frac{S-1}{\left(\frac{L_v}{R_v T} - 1\right)\frac{L_v \rho_l}{f_h K T} + \frac{\rho_l R_v T}{f_v D_v e_s(T)}} \tag{4}$$

following Pruppacher and Klett (1978) and Rogers and Yau (1989). In (4), S is the saturation ratio, L_v is the latent heat of vaporization, R_v is the gas constant for water vapor, T is the air temperature, ρ_l is the density of liquid water, K and D_v are the thermal conductivity of air and diffusivity of water vapor, respectively, $e_s(T)$ is the saturation vapor pressure as a function of T, and f_v and f_h are the ventilation coefficients for vapor and heat, as in Pruppacher and Klett (1978) and Rasmussen and Heymsfield (1987). The functional dependence of L_v, K, D_v, and $e_s(T)$ on temperature can be found in Rasmussen and Heymsfield (1987).

We are interested in the vertical profiles of the polarimetric variables, so we convert (4) into an expression for the change in radius with height dr/dh. To simplify the ensuing integration, the empirical power law fall speed relation suggested by Atlas and Ulbrich (1977) is used for the terminal velocity of the raindrops

$$v(D) = \alpha D^{\beta} \tag{5}$$

where $\alpha = 3.78$ m s^{-1} mm$^{-0.67}$ and $\beta = 0.67$, where the equivalent spherical diameter D is given in mm. Thus, performing the change of variables in equation (4) and using the velocity relation in (5) yields an analytic expression for the change in diameter of a raindrop with initial size D_0 as a function of height

$$D(h) = \left[D_0^{\beta+2} + \frac{4\xi \Delta h(\beta+2)}{\alpha} \right]^{\frac{1}{\beta+2}} \tag{6}$$

where we have defined ξ as the right hand side of equation (4), which is assumed constant over each height interval Δh. The change in diameter of the size bins at each height level and an assumed initial DSD aloft are used to compute the vertical profiles of polarimetric variables according to the T-Matrix method of Mishchenko (2000). The raindrops are assumed to have a distribution of canting angles with mean 0° and standard deviation 20°.

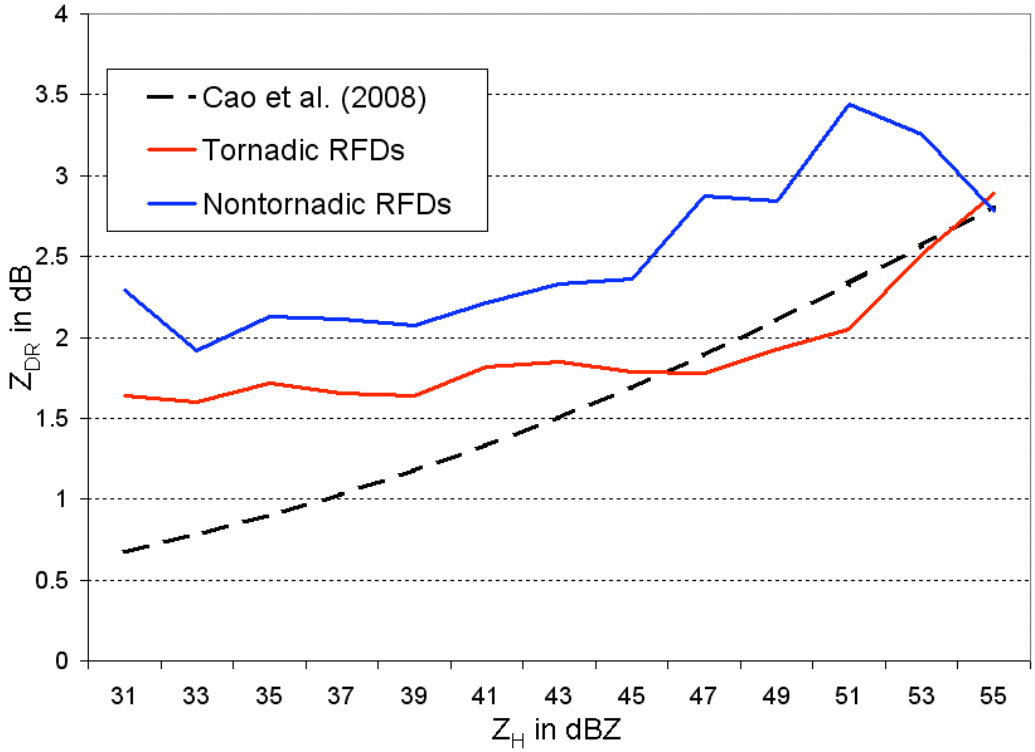

Fig 6: Median lines for tornadic (red) and nontornadic (blue) Z_{DR} compared to the observed Oklahoma $Z_H - Z_{DR}$ relation suggested by Cao et al. (2008) in the dashed black line.

4.2. Experimental Design

The polarimetric measurements presented in the previous section suggest that the DSD in supercell hook echoes is unusual. Unfortunately, extremely limited observational data can be found in the literature. To the knowledge of the authors, only one study has directly measured the DSD in a supercell storm using a 2D video disdrometer (Schuur et al. 2001). As expected, very large drops (> 5 mm) were observed beneath the part of the storm where the Z_{DR} arc is found. In the core of the supercell, Schuur et al. (2001) found a larger concentration of very small drops (< 1 mm) than in the other cases they investigated. Albeit anecdotal evidence, the first author and several scientists and storm chasers he has talked to have experienced large quantities of tiny drops while driving through supercell hook echoes[1]. Therefore, though the polarimetric variables indicate a preponderance of larger drops, other observations suggest that a large concentration of tiny drops may be present as well.

Any DSD can be prescribed in the model. In addition to the conventional exponential and gamma models, a bi-exponential model is also examined (7).

$$N(D) = N_0 \exp(-\Lambda_0 D) + N_1 \exp(-\Lambda_1 D) \qquad (7)$$

The bi-exponential model (herein BX) parameters were selected experimentally with the following requirements: (i) the DSD must have a large concentration of small drops, (ii) the DSD must produce values of the polarimetric variables consistent with observations. To satisfy these requirements (Z_H ~ 33 dBZ, Z_{DR} ~ 2 dB), the parameters are set at N_0 = 9000 m^{-3} mm^{-1}, Λ_0 = 3.58 mm^{-1}, N_1= 10 m^{-3} mm^{-1}, and Λ_1 = 1.3 mm^{-1}. A Marshall-Palmer DSD (herein MP) was used for the exponential model, and the gamma models were constrained based on observed Z_H and Z_{DR} values following Zhang et al. (2001, 2006), Brandes et al. (2004), and Cao et al. (2008). One gamma model uses a $\mu > 0$ (denoted as Γ^+) and the other uses a $\mu < 0$ (Γ^-), which is more frequently observed in convective storms (Guifu Zhang, personal communication 2008). Table 2 provides the parameters for each modeled DSD.

Considerable work has been done in quantifying the rate of evaporation in different thermodynamic conditions and its impact on conventional radar rainfall estimates (e.g., Li and Srivastava 2001), evolution of DSD shape (e.g., Hu and Srivastava 1995), production of downdrafts (e.g., Srivastava 1985, 1987) and even supercell evolution (e.g., Gilmore and Wicker 1998), so we focus on the response of the polarimetric variables

[1] For example, personal communication with Jerry Straka (2008), Alex Schenkman (2008), Robin Tanamachi (2008), Gabriel Garfield (2007), Don Giuliano (2007) and Corey Potvin (2007).

DSD	N_0	N_1	Λ_0	Λ_1	μ
BX	9000	10	3.58	1.3	---
MP	8000	---	3.06	---	---
Γ^+	500	---	2.2	---	0.169
Γ^-	300	---	1.9	---	-0.07

Table 2: Parameters for the four DSD models used in the simulations. The names represent the bi-exponential DSD (BX), the Marshall-Palmer inverse exponential DSD (MP), and the Gamma DSD with $\mu > 0$ and $\mu < 0$ (Γ^+ and Γ^-, respectively). The values of N_0 and N_1 have units $mm^{-1}\ m^{-3}$; Λ_0 and Λ_1 have units mm^{-1}; μ is dimensionless.

at S band and C band. We define the "evaporative change" as the change in the polarimetric variables due to evaporation as drops fall 3 km through the subsaturated domain, denoted by a Δ before the polarimetric parameter. The value at the ground is subtracted from the initial value at the top of the domain, but the absolute value is taken for ΔZ_{DR}.

The first three sets of experiments test the sensitivity of the model. First, we investigate the sensitivity of the evaporative change in polarimetric variables to changes in relative humidity and lapse rate. The second set of experiments holds relative humidity constant at 75% and varies the lapse rate from 0 (i.e., isothermal) to 10 °C km^{-1} (approximately dry adiabatic), with a surface temperature of 20°C in each case. Again these are performed for each of the four DSD models. In the next set of sensitivity tests, we quantify the impact of changing the initial DSD parameters for the exponential model. It is well known that the slope of the MP DSD (with $N_0 = 8000\ mm^{-1}\ m^{-3}$) can be described in terms of the rainfall rate R through the relation $\Lambda = 4.1R^{-0.21}$ (e.g., Doviak and Zrnić 1993). The next set of sensitivity tests varies R from 1 mm hr^{-1} to 400 mm hr^{-1} using the MP DSD for a dry adiabatic environment with a constant relative humidity of 75% and a surface temperature of 30 °C. The intercept parameter N_0 is held constant at 8000 $mm^{-1}\ m^{-3}$.

After the sensitivity tests, the model is used to simulate evaporation in supercell environments. The lowest 3 km of soundings from each of the nine supercell cases (see Table 1) are used to prescribe the temperature and relative humidity profiles in the model. For each case the 00 UTC Norman, Oklahoma (OUN) sounding is used. Vertical profiles of Z_H, Z_{DR}, K_{DP}, and ρ_{HV} are constructed.

4.3. Simulation Results and Analysis

In general, the sensitivity tests confirmed what is expected intuitively and thus for brevity the results will not be shown, with the exception of a few key points. At both S and C bands, ΔZ_H is significantly greater for the MP model than the other DSDs. Similarly, ΔK_{DP} is largest for the MP DSD, though the difference is less significant (relative to the other DSD models) than for ΔZ_H. The values of ΔK_{DP} at C band are about twice as large as at S band. The largest ΔZ_{DR} occurs for the BX model, which shows a substantially larger evaporative change in Z_{DR} than the other models. The differences are all enhanced at C band, but only slightly for the MP model. At S band, the $\Delta\rho_{HV}$ is insignificant for all DSD models, though it becomes about an order of magnitude larger for the gamma models at C band. The relatively large discrepancies between the experimental DSDs reveal the importance of selecting the most representative model and highlight the problem of uncertainty regarding the true DSDs in supercells.

When varying the intercept parameter of the MP distribution, the evaporative change in Z_H, Z_{DR}, and ρ_{HV} remain constant. However, ΔK_{DP} increases approximately linearly with increasing N_0. This is because raising N_0 increases the total number concentration of drops. Whereas Z_{DR} and ρ_{HV} are independent of total concentration, K_{DP} is the polarimetric variable most strongly affected by concentration of raindrops.

The results of varying the rainfall rate are provided in Fig. 7. Interestingly, ΔK_{DP} increases and ΔZ_H decreases for increasing R. Since K_{DP} is approximately linearly related to R, it follows that ΔK_{DP} is also linearly proportional to R. Thus, for heavy rain events with high Z_H, one should expect a greater change in K_{DP} for a given amount of evaporation than is observed in Z_H. At C band, ΔK_{DP} for a given R is about twice as large as ΔK_{DP} at S band. In general, ΔZ_{DR} decreases with increasing R for both S and C bands. This is because heavier rain is characterized by higher concentrations of large drops (at least for the MP model), so the reduction of small drops by evaporation has a smaller relative change in the median drop size of the distribution. For both S and C bands, the evaporative change in ρ_{HV} is insignificant for all rainfall rates for the MP model.

Despite the oversimplified model and the inherent sampling and representativeness issues of supercell proximity soundings, two cases are selected to offer a means of comparison for the simulations. In an attempt to isolate thermodynamic effects that may impact tornadogenesis from those due to low-level wind shear, the tornadic and nontornadic cases with the most similar 0 – 3 km hodographs are selected: 31 March 2008 and 1 June 2008. Surprisingly, the dewpoint temperature profile for both cases is fairly similar,

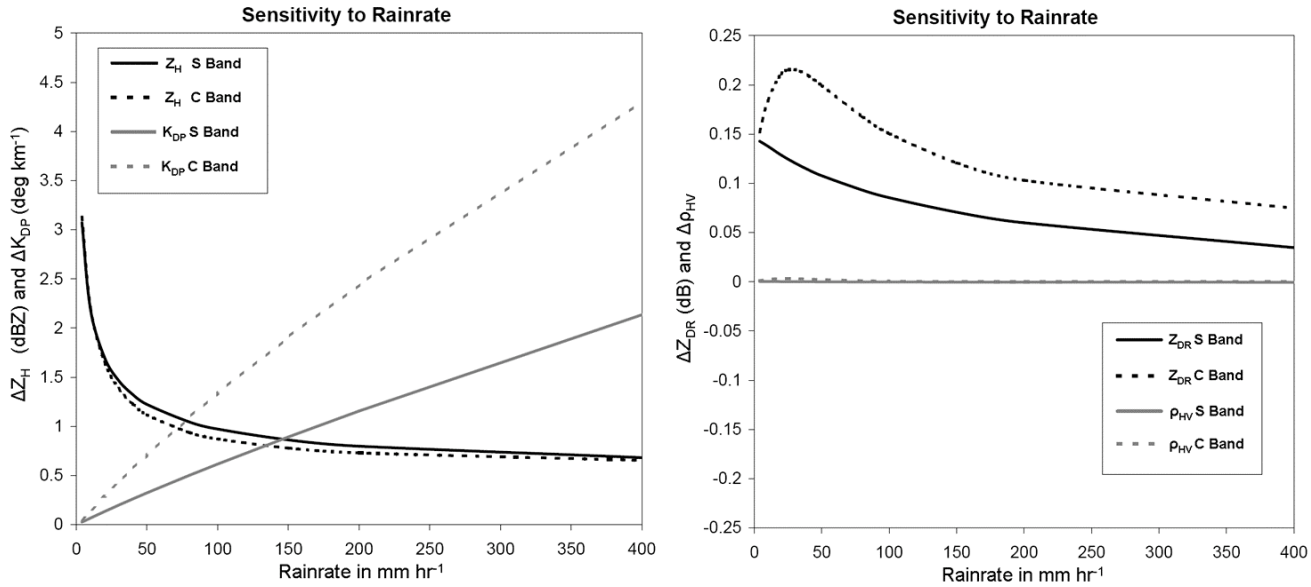

Fig. 7: Sensitivity of the evaporative change in the polarimetric variables to rainfall rate for a MP DSD. The environment is dry adiabatic with a constant profile of RH=75%. S-band values are shown in solid lines and C-band values are in dashed lines. In the left panel, ΔZ_H (black) and ΔK_{DP} (gray) are shown. In the right panel, black represents ΔZ_{DR} and gray represents $\Delta \rho_{HV}$.

though the temperature in the 1 June case is on average 6 °C warmer than the 31 March case, resulting in lower relative humidity. The BX model is used for the simulation to try to capture the exotic characteristics of DSD in RFDs. The resulting vertical profiles of polarimetric variables for the two cases reveal more evaporation occurring in the nontornadic case (Fig. 8). Because it is only a single comparison between two cases, one should be cautious and not make any generalizations. The important result is that the magnitude of the difference between the polarimetric variables at the surface, especially Z_{DR}, is in agreement with the observations from Section 3. At S band, the simulation has the nontornadic environment producing a Z_{DR} value at the surface 0.3 dB greater than the tornadic case for the same initial DSD, compared to the observed median difference between tornadic and nontornadic RFDs of about 0.5 dB. At C band, the modeled difference is larger, in agreement with the sensitivity experiments. For both cases, the change in ρ_{HV} is quite small, with the nontornadic case resulting in *higher* ρ_{HV} than the tornadic case. As we have seen, however, this is dependent on the choice of DSD used in the simulations and is not expected to be important at S band.

4.4. Discussion of Resonance Scattering Effects

The results above indicate differences in ρ_{HV} observed at S band between T and NT storms due to differing rates of evaporation are insignificant. Contributions from resonance-sized scatterers can substantially decrease the measured ρ_{HV}. For an hydrometeor with dielectric constant ε, diameter D, and an incident electromagnetic wave with wavelength λ, the first resonance scattering effects occur when the resonance parameter

$$\Re = \frac{D\sqrt{|\varepsilon|}}{\lambda} \qquad (9)$$

approaches unity (Kumjian and Ryzhkov 2008). The decrease in ρ_{HV} comes partly from the contribution of scatterers with nonzero backscatter differential phase δ in the sampling volume; the backscatter differential phase shift is nonzero for scatterers with $\Re > 0.5$. At S band, δ only becomes nonzero for drops larger than about 6 mm, which are comparatively sparse in most natural DSDs. The observed ρ_{HV} will be minimized when the relative contribution from these larger drops becomes more significant, which can occur in situations such as size sorting (e.g., Kumjian and Ryzhkov 2009) and when smaller drops are depleted by vigorous evaporation.

Resonance scattering effects are more important for C-band radars, since the resonance parameter approaches unity for liquid raindrops about 4 – 6 mm in diameter, a size commonly found in convective storms originating from melted hail and graupel. In fact, ρ_{HV} can drop as low as about 0.93 in pure rain at C band. Thus, any changes in the relative contribution from these large drops within the radar sampling volume (e.g., due to size sorting, evaporation) have a more pronounced effect on the measured ρ_{HV} and Z_{DR}.

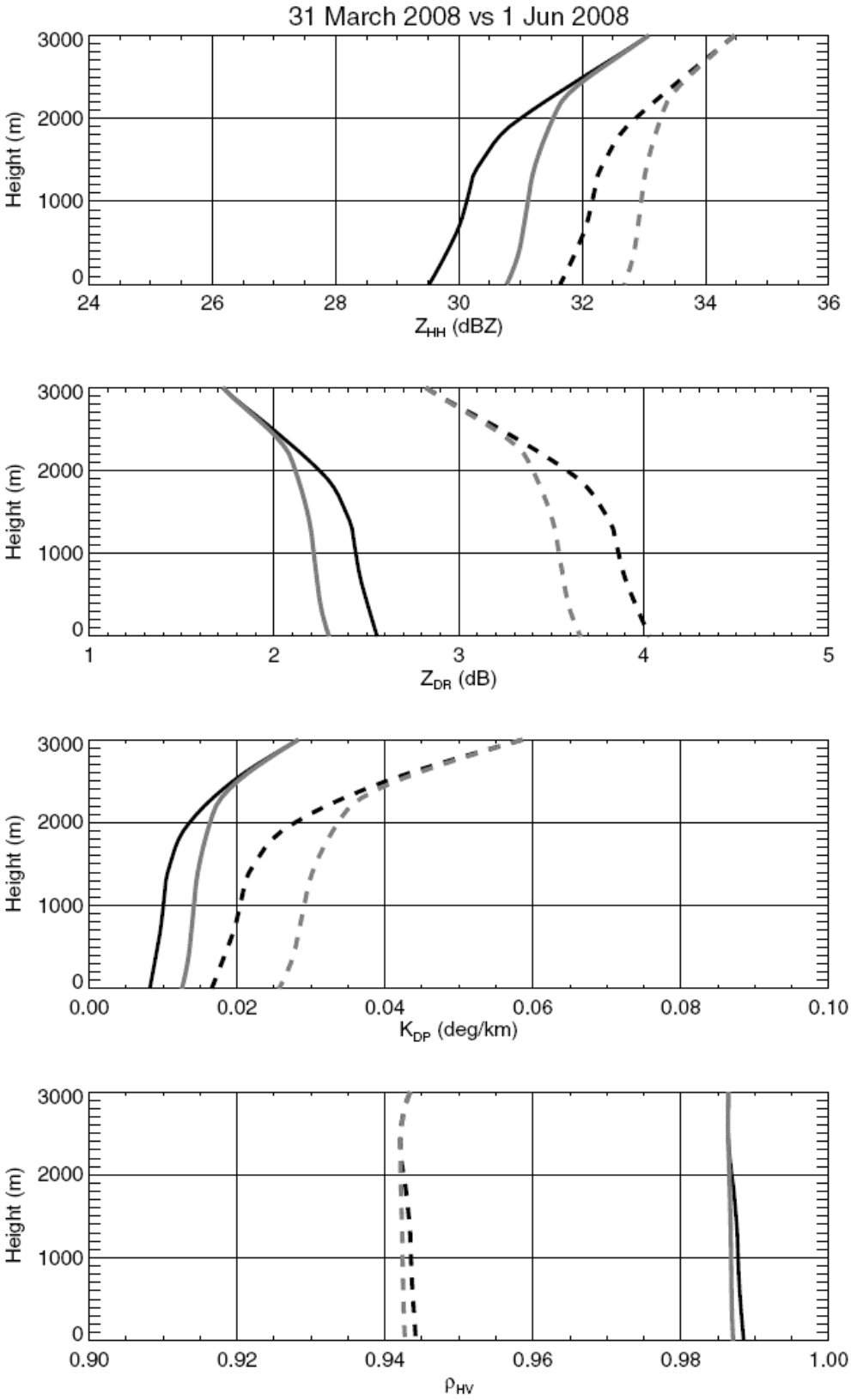

Fig. 8: Comparison of model simulations for a nontornadic case (1 June 2008, black lines) and a nontornadic case (31 March 2008, gray lines). S-band values are shown in solid lines, C-band in dashed lines.

5. CONCLUSIONS

The impact of evaporation of raindrops on the polarimetric variables is quantified. In addition to being sensitive to thermodynamic conditions, the magnitude of the changes in polarimetric variables is dependent on factors such as the choice of DSD model and rainfall rate. At S band, changes in ρ_{HV} were found to be insignificant. At C band, however, the changes are more substantial, though the direction of the change is dependent on the initial DSD aloft.

Further in situ measurements in supercells are required to better understand the relative importance of evaporation to other microphysical processes such as melting, size sorting, drop breakup, collisions, and coalescence. Do supercells consistently display the same type of DSD? Owing to the spectrum of supercells observed (e.g., HP to LP; see Moller et al. 1994), considerable variability in the DSDs of supercell storms may exist.

Subtle differences in the polarimetric characteristics of tornadic and nontornadic supercell hook echoes are found. Nontornadic storms apparently have DSDs skewed towards larger drops, consistent with previous research suggesting that the rates of evaporative cooling and the resulting low-level thermodynamic characteristics of the RFD may have an impact on tornadogenesis (Markowski et al. 2002, 2003). The model results in section 4 show that such subtle differences at S band in Z_{DR} for a given Z_H are consistent with those that can be attributed to differences in evaporative cooling. At S band the difference in ρ_{HV}, albeit very small in magnitude, cannot be attributed to evaporation. If the difference is not simply a statistical artifact owing to small sample size, other factors must be considered. For example, an increased prevalence of small melting hail in nontornadic hook echoes could decrease the observed ρ_{HV} and increase the Z_{DR} relative to the observed values in tornadic hook echoes. The melting of small hail can significantly contribute to the negative buoyancy in convectively-driven downdrafts (e.g., Srivastava 1987), which would favor colder RFDs and tornadogenesis failure. We rule out the possibility that lower Z_{DR} in tornadic hook echoes is from the presence of hail more frequently than in nontornadic hook echoes because of the relatively high ρ_{HV}.

From the current dataset there are no apparent differences in the measured $R(Z_H)$ and $R(K_{DP})$ between tornadic and nontornadic hook echoes. A comparison of the observed rainfall rates suggests that in general the DSDs in supercell hook echoes are skewed towards larger drops more than in other precipitation systems.

Observations of the differences at S band presented in this paper are subtle and have considerable statistical uncertainty. Thus, operational or real-time discrimination between tornadic and nontornadic supercells with S-band polarimetric radars may not be practical. However, the theoretical and modeling results presented above indicate that these differences should be amplified at C band due to the resonance scattering effects present at shorter wavelengths. The effects at X band may not be as amplified due to greater attenuation, which acts to damp out the effects of resonance scattering. Operational applications of these findings may be more practical for systems of C-band polarimetric radars, such as those found in Europe. A similar investigation of data at C band is necessary to refute or verify this possibility.

Traditional modeling approaches fit DSDs to known mathematical models such as the exponential or constrained gamma model. However, the polarimetric measurements presented in this study suggest that the true DSD in supercells may be quite exotic, not conforming to commonly-used analytic models. In this case, polarimetric radar measurements can be used to retrieve information about the DSD, which may be used for short-term simple explicit microphysics models of processes such as evaporation (like the one constructed for this study). This type of modeling approach may be used to predict low-level thermodynamic conditions that may give guidance for short-term forecasts of the potential for tornadogenesis in supercells.

6. ACKNOWLEDGEMENTS

We would like to thank the NSSL/CIMMS employees who maintain and operate KOUN for their time and effort that ensures the research-grade quality of the radar and its data. This work is partially funded under the NSF Grant ATM-0532107 and under the NOAA/University of Oklahoma Cooperative Agreement NA17RJ1227, U.S. Department of Commerce.

7. REFERENCES

Atlas, D. and C.W. Ulbrich, 1977: Path- and area-integrated rainfall measurement by microwave attenuation in the 1 – 3 cm band. *J. Appl. Meteor.*, **16**, 1322-1331.

Battan, L.J., 1959: *Radar Meteorology*. The University of Chicago Press, 161 pp.

Brandes, E.A. 1981: Finestructure of the Del City-Edmond tornadic meso-circulation. *Mon. Wea. Rev.*, **109**, 635-647.

Brandes, E.A., G. Zhang, and J. Vivekanandan, 2004: Drop size distribution retrieval with polarimetric radar: Model and application, *J. Appl. Meteor.* **43**, 461–475.

Bringi, VN and V. Chandrasekar, 2001. *Polarimetric Doppler Weather Radar*. Cambridge University Press, 336 pp.

Cao, Q., G. Zhang, E. Brandes, T. Schuur, A.V. Ryzhkov, and K. Ikeda, 2008: Analysis of video disdrometer and polarimetric radar data to characterize rain microphysics in Oklahoma. *J. Appl. Meteor. and Climatology*, **47**, 2238-2255.

Davies-Jones, R. P., 1982: A new look at the vorticity equation with application to tornadogenesis. Preprints, *12th Conf. on SevereLocal Storms,* San Antonio, TX, Amer. Meteor. Soc., 249–252.

Davies-Jones, R.P., 2008: Can a descending rain curtain in a supercell instigate tornadogenesis barotropically? *J. Atmos. Sci.*, **65,** 2469-2497**.**

Davies-Jones, R.P. and H.E. Brooks, 1993: Mesocyclogenesis from a theoretical perspective. *The Tornado: Its Structure, Dynamics, Prediction, and Hazards. Geophys. Monogr.*, No. 79, Amer. Geophys. Union, 105-114.

Giangrande, S.E., J.M. Krause, and A.V. Ryzhkov, 2008: Automatic designation of the melting layer with a polarimetric prototype of the WSR-88D radar. *J. Appl. Meteor. and Climatology,* **47**, 1354-1364**.**

Gilmore, M.S., and L.J. Wicker, 1998: The influence of midtropospheric dryness on supercell morphology and evolution. *Mon. Wea. Rev.*, **126**, 943–958.

Grzych, M.L., B.D. Lee, and C.A. Finley, 2007: Thermodynamic analysis of supercell rear-flank downdrafts from project ANSWERS. *Mon. Wea. Rev.*, **135**, 240-246.

Hu, Z., and R. Srivastava, 1995: Evolution of raindrop size distribution by coalescence, breakup, and evaporation: Theory and observations. *J. Atmos. Sci.*, **52**, 1761–1783.

Klemp, J.B. and R, Rotunno, 1983: A study of the tornadic region within a supercell thunderstorm. *J. Atmos. Sci.*, **40**, 359-377.

Kumjian, M.R. and A.V. Ryzhkov, 2008: Polarimetric signatures in supercell thunderstorms. *J. Appl. Meteor. and Climatology*, **47**, 1940-1961.

Kumjian, M.R. and A.V. Ryzhkov, 2009: Storm-relative helicity revealed from polarimetric radar measurements. *J. Atmos. Sci.*, **in press**.

Lemon, L.R., and C.A. Doswell, 1979: Severe thunderstorm evolution and mesocyclone structure as related to tornadogenesis. *Mon. Wea. Rev.*, **107**, 1184-1197.

Li, X., and R.C. Srivastava, 2001: An analytical solution for raindrop evaporation and its application to radar rainfall measurements. *J. Appl. Meteor.*, **40**, 1607–1616.

Ludlam, F. H., 1963: Severe Local Storms: A review. *Severe Local Storms, Meteor. Monogr.,* No. 27, 1–30.

Markowski, P.M., 2002: Hook echoes and rear-flank downdrafts: A review. *Mon. Wea. Rev.*, **130**, 852-876.

Markowski, PM, J. Straka, and E Rasmussen, 2002: Direct surface thermodynamic observations within the rear-flank downdrafts of nontornadic and tornadic supercells. *Mon. Wea. Rev.*, **130**, 1692-1721.

Markowski, P.M., J.M. Straka, and E.N. Rasmussen, 2003: Tornadogenesis resulting from the transport of circulation by a downdraft: Idealized numerical simulations. *J. Atmos. Sci.*, **60**, 795-823.

Markowski, P.M., E.N. Rasmussen, J.M. Straka, R.P. Davies-Jones, and Y. Richardson, 2008: Vortex lines within low-level mesocyclones obtained from pseudo-dual-Doppler radar observations. *Mon. Wea. Rev.*, **136**, 3513-3535.

Mishchenko, M.I. 2000: Calculation of the amplitude matrix for a nonspherical particle in a fixed orientation. *Appl. Optics*, **39**, 1026-1031.

Moller, A.R., C.A. Doswell, M.P. Foster, and G.R. Woodall, 1994: The operational recognition of supercell thunderstorm environments and storm structures. *Wea. Forecasting*, **9**, 327–347.

Pruppacher, H.R. and J.D. Klett, 1978: *Microphysics of Clouds and Precipitation*, 2nd ed. Oxford University Press, 953 pp.

Rasmussen, E.N., J.M. Straka, R.P. Davies-Jones, C.A. Doswell III, F.H. Carr, M.D. Eilts, and D.R. MacGorman, 1994: The Verifications of the Origins of Rotation in Tornadoes Experiment: VORTEX. *Bull. Amer. Meteor. Soc.*, **75**, 997-1006.

Rasmussen, RM and A.J. Heymsfield, 1987: Melting and shedding of graupel and hail. Part I: Model physics. *J. Atmos. Sci.*, **44**, 2754-2763

Rogers, R.R. and M.K. Yau, 1989: *A Short Course in Cloud Physics*, 3rd ed. Elsevier Press, 290 pp.

Rotunno, R. and J. Klemp, 1982: The influence of the shear-induced pressure gradient on thunderstorm motion. *Mon. Wea. Rev.*, **110**, 136-151.

Ryzhkov, A.V., T.J. Schuur, D.W. Burgess, P.L. Heinselman, S.E. Giangrande, and D.S. Zrnić, 2005a: The joint polarization experiment. *Bull. Amer. Meteor. Soc.*, **86**, 809-824.

Ryzhkov, A.V., T.J. Schuur, D.W. Burgess, and D.S. Zrnić, 2005b: Polarimetric tornado detection. *J. Appl. Meteor.*, **44**, 557-570.

Ryzhkov, A.V. and D.S. Zrnić, 1996: Assessment of Rainfall Measurement That Uses Specific Differential Phase. *J. Appl. Meteor.*, **35**, 2080–2090.

Schuur, T.J., A.V. Ryzhkov, D.S. Zrnić, and M. Schönhuber, 2001: Drop size distributions measured by a 2D video disdrometer: Comparison with dual-polarization radar data. *J. Appl. Meteor.*, **40**, 1019-1034.

Shapiro, A., 2005: Drag-induced transfer of horizontal momentum between air and raindrops. *J. Atmos. Sci.*, **62**, 2205–2219.

Srivastava, R., 1985: A simple model of evaporatively driven dowadraft: Application to microburst downdraft. *J. Atmos. Sci.*, **42**, 1004–1023.

Srivastava, R., 1987: A model of intense downdrafts driven by the melting and evaporation of precipitation. *J. Atmos. Sci.*, **44**, 1752–1774.

Straka, J.M., E.N. Rasmussen, and S.E. Fredrickson, 1996: A mobile mesonet for finescale meteorological applications. *J. Atmos. Oceanic Technol.*., **13,** 921-936.

Straka, J.M., D.S. Zrnić, and A.V. Ryzhkov, 2000: Bulk hydrometeor classification and quantification using polarimetric radar data: synthesis of relations. *J Appl. Meteor.*, **39**, 1341-1372.

Trapp, R.J., 1999: Observations of nontornadic low-level mesocyclones and attendant tornadogenesis failure during VORTEX. *Mon. Wea. Rev.*, **127**, 1693-1705.

Wakimoto, R.M., and H. Cai, 2000: Analysis of a nontornadic storm during VORTEX 95. , **128**, 565–592.

Wakimoto, R.M., C. Liu, and H. Cai, 1998: The Garden City, Kansas, Storm during VORTEX 95. Part I: Overview of the storm's life cycle and mesocyclogenesis. , **126**, 372–392.

Wicker, L.J. and R.B. Wilhelmson, 1995: Simulation and analysis of tornado development and decay within a three-dimensional supercell thunderstorm. *J. Atmos. Sci.*, **52**, 2675-2703.

Zhang, G., J. Vivekanandan, and E. Brandes, 2001: A method for estimating rain rate and drop size distribution from polarimetric radar measurements. *IEEE Trans. Geosci. Remote Sens.,* **39,** 830–841.

Zhang, G., J. Sun, and E.A. Brandes, 2006: Improving parameterization of rain microphysics with disdrometer and radar observations. *J. Atmos. Sci.*, **63**, 1273–1290.

Zrnić, D.S. and A.V. Ryzhkov, 1999: Polarimetry for weather surveillance radars. *Bull. Amer. Meteor. Soc.*, **80**, 389-406.